Bioconjugate Chemistry

Article

pubs.acs.org/bc

Effects of Nanoparticle Size on Multilayer Formation and Kinetics of Tethered Enzymes

James P. Lata,[†,‡] Lizeng Gao,[†] Chinatsu Mukai,[†] Roy Cohen,[†] Jacquelyn L. Nelson,[†] Lynne Anguish,[†] Scott Coonrod,[†] and Alexander J. Travis*[,†,‡,§]

[†]Baker Institute for Animal Health, [‡]Biomedical Engineering, and [§]Atkinson Center for a Sustainable Future, Cornell University, , Ithaca, New York 14853, United States

Supporting Information

ABSTRACT: Despite numerous applications, we lack fundamental understanding of how variables such as nanoparticle (NP) size influence the activity of tethered enzymes. Previously, we showed that biomimetic oriented immobilization yielded higher specific activities versus nonoriented adsorption or carboxyl-amine binding. Here, we standardize NP attachment strategy (oriented immobilization via hexahistidine tags) and composition (Ni-NTA coated gold NPs), to test the impact of NP size (⌀5, 10, 20, and 50 nm) on multilayer formation, activity, and kinetic parameters (k_{cat}, K_M, k_{cat}/K_M) of enzymes representing three different classes: glucose-6-phosphate isomerase (GPI), an isomerase; Glyceraldehyde-3-phosphate dehydrogenase S (GAPDHS), an oxidoreductase; and pyruvate kinase (PK), a transferase. Contrary to other reports, we observed no trend in kinetic parameters for individual enzymes when found in monolayers (<100% enzyme coverage), suggesting an advantage for oriented immobilization versus other attachment strategies. Saturating the NPs to maximize activity per NP resulted in enzyme multilayer formation. Under these conditions, total activity per NP increased with increasing NP size. Conversely, specific activity for all three enzymes was highest when tethered to the smallest NPs, retaining a remarkable 73−94% of the activity of free/untethered enzymes. Multilayer formations caused a clear trend of k_{cat} decreasing with increasing NP size, yet negligible change in K_M. Understanding the fundamental relationships between NP size and tethered enzyme activity enables optimized design of various applications, maximizing activity per NP or activity per enzyme molecule.

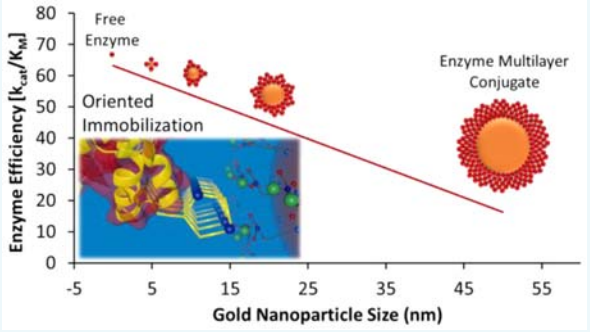

INTRODUCTION

NPs have many positive attributes for use in biotechnological applications, including dispersibility, high surface area, and the ability to be integrated into various devices with spatial control. Applications for NPs with attached enzymes include biocatalysis,[1] biosensing,[2] biofuel cells,[3] disease diagnosis,[4] and drug delivery.[5] Because enzyme attachment can block substrate binding sites or interfere with necessary conformational changes,[6] much attention has focused on surface attachment chemistry.[7] However, other variables can also exert profound influences on tethered enzyme function, but surprisingly have been rarely studied.

Surface composition, geometry, roughness, porosity, and subnanometer morphology can all impact surface modifications and/or enzyme binding.[8,9] In addition, surface charge can have dramatic effects on the enzymes bound.[10,11] Characteristics of the medium in which the conjugates are suspended such as pH, temperature, viscosity, and salt concentrations can also impact enzyme function.[12,13] Many enzymes form functional multimers and can bind with one another to create multilayers, dependent on protein surface charge, size, tertiary and quaternary structure, and packing density. Multilayer formation and tethered enzyme activity can also be affected by NP size and surface area, thereby affecting the performance of functionalized NPs across diverse applications. Despite this fundamental importance, there has been relatively little study of the effect of NP size on the function of different types of immobilized enzymes.

The few notable studies investigating the effects of NP size on activity have typically utilized single enzymes at less than 50% surface coverage. The many technical differences among these studies resulted in varying findings regarding K_M, k_{cat}, and specific activity (SI Table 1).[11,13−15] These studies were all limited to single enzymes and used attachment strategies, such as nonspecific binding or chemically specific but nonoriented binding, which are suboptimal for retaining enzymatic activity. Coupled with the use of different NPs of different size ranges, as well as use of varying measurements to quantify activity, these differences limit one's ability to draw generalizable conclusions about the impact of NP size on function. To date, no reports have provided fundamental understanding of the impacts of NP size on the activity of multiple enzyme classes

Received: June 26, 2015
Revised: August 11, 2015
Published: August 17, 2015

DOI: 10.1021/acs.bioconjchem.5b00354
Bioconjugate Chem. 2015, 26, 1931−1938

standardizing surface attachment chemistry, NP composition, and kinetic analysis, with consideration of multilayer formation under conditions of maximal enzyme loading. This aspect is critical for practical application of these technologies, as maximum function per NP reduces the overall amount of NPs needed.

Previously, we showed that biomimetic oriented immobilization yielded higher specific activities versus nonoriented adsorption or carboxyl-amine binding.[16,17] Here, we standardized NP attachment strategy (oriented immobilization via hexahistidine tags) and composition (Ni-NTA coated gold NPs), to test the impact of NP size (⌀5, 10, 20, and 50 nm) on multilayer formation, activity, and kinetic parameters (k_{cat}, K_M, k_{cat}/K_M) of enzymes representing three different classes: glucose-6-phosphate isomerase (GPI), an isomerase; glyceraldehyde-3-phosphate dehydrogenase S (GAPDHS), an oxidoreductase; and pyruvate kinase (PK), a transferase.

To standardize surface attachment chemistry to the NP, we chose oriented immobilization using genetically encoded hexahistidine tags (His-tag). Unlike random adsorption, or chemically specific but nonoriented approaches such as carboxyl-amine binding (the two most common approaches), genetically positioned binding tags facilitate immobilization in a specific orientation. This reduces the impact of subtle (sub-nm) morphological surface variation and the parts of the protein that come into direct contact with the surface, a common problem with nonspecific adsorption of enzymes.[11] Unlike the more common binding approaches, genetically encoded tags can be positioned to allow access to the substrate binding domain and any needed conformational changes.[18,19] In our previous studies,[16,17] we showed that this strategy led to higher specific activities than the same enzymes when randomly adsorbed or attached via carboxyl-amine binding.

RESULTS AND DISCUSSION

We chose three mammalian glycolytic enzymes, each representing a different enzyme class, and genetically engineered them to include an N-terminal His-tag (Figure 1).

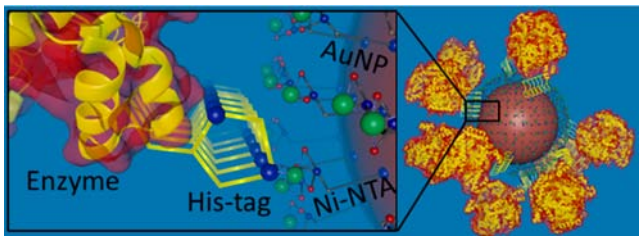

Figure 1. Site-specific, oriented immobilization for the binding of enzymes to AuNPs. This schematic representation shows a genetically engineered enzyme with an N-terminal his-tag bound to Ni-NTA groups on a AuNP surface. The genetically encoded binding tag is positioned to replace a putative germ cell-specific binding domain (where applicable) with the goal being to minimize impact on substrate binding, needed conformational changes, and steric hindrance.

GPI isomerizes glucose-6-phosphate into fructose-6-phosphate. GAPDHS converts glyceraldehyde 3-phosphate to D-glycerate 1,3-bisphosphate through a coupled phosphorylation/oxidation reaction with NAD^+. PK catalyzes the conversion of phosphoenolpyruvate to pyruvate through phosphorylation of ADP into ATP. All three enzymes were reverse transcribed from mouse testis RNA. A germ cell-specific, proline-rich domain of GAPDHS[20] was replaced with the His-tag. Enzymes were expressed, purified, and first tested for activity when free in solution prior to immobilization on AuNPs (data not shown).

AuNPs have many attractive properties which make them ideal as a binding support including high dispersibility, biocompatibility, and high stability at small scales. We modified AuNPs (⌀5, 10, 20, and 50 nm; Sigma) with Ni-NTA (NTA-AuNP), and verified size using SEM (SI Figure 1). We measured the zeta potentials of each size before and after modification, finding lower AuNP aggregation[21−23] after modification (Zetasizer Nano ZS, Malvern; SI Figure 2). We first evaluated a monolayer of enzyme tethered to each size of NTA-AuNP with less than 100% AuNP coverage. Absorbance values were used to calculate NTA-AuNP concentrations, which were used in standardizing the NTA-AuNPs to equal surface area (SI Figure 3). A sufficient amount of enzyme to create a monolayer was incubated with NTA-AuNPs of each size and then washed repeatedly. Amounts of enzyme bound and the percent of each AuNP covered (SI Figure 4) were measured/calculated by performing BCA assays on each wash and subtracting the total unbound from the initial protein amount (SI Figure 5).

After assessing binding, each conjugate preparation was utilized in side-by-side activity and kinetic assays. Kinetic measurements were obtained using coupled reactions linked to the reduction of NAD^+ to NADH (GAPDHS) or $NADP^+$ to NADPH (GPI), or the oxidation of NADH to NAD^+ (PK). Reactions were carried out in 96-well plates and absorbance read at 340 nm. Measurements for each enzyme at each AuNP size were carried out in triplicate. The second enzymatic step for each reaction was tested with NTA-AuNPs in suspension to rule out any change in signal due to the presence of NPs, as well as verifying that these enzymes were not limiting the reaction rate (Supplementary Figure 6). The three kinetic variables we evaluated were k_{cat}, K_M, and k_{cat}/K_M (Figure 2). We also evaluated activity per NP (Supplementary Figure 7), finding that larger NPs, covered with more enzymes, had higher activities.

The turnover number (k_{cat}) is the maximum number of substrate molecules converted to product per enzyme molecule per second. As expected, each enzyme had varying inherent turnover numbers for the free enzymes (not tethered), ranging from GPI at 108.5 s^{-1} to GAPDHS at 15.7 s^{-1}. Although statistically significant differences in k_{cat} were noted in individual comparisons among sizes for all three enzymes when tethered as monolayers (Figure 2), we are cautious about over-interpreting these differences due to the fact that the NPs were standardized according to surface area; this resulted in increased numbers of larger NPs being used, making them slightly more susceptible to loss during washing. Given this situation, the subtle differences we noted were not that dissimilar to observations from previous studies showing no clear changes in k_{cat}.[13,14]

K_M inversely relates to substrate affinity. For all three enzymes, immobilization did not confer any significant, generalizable changes in K_M. Previous studies using nonspecific adsorption[14] and random amine binding techniques[13] suggested that K_M varied with NP size. This discrepancy is likely because our use of oriented immobilization reduced the likelihood of blocking the substrate binding domain and helped prevent the enzyme from coming into direct contact with the surface. Our findings suggest that prior results were dependent

DOI: 10.1021/acs.bioconjchem.5b00354
Bioconjugate Chem. 2015, 26, 1931−1938

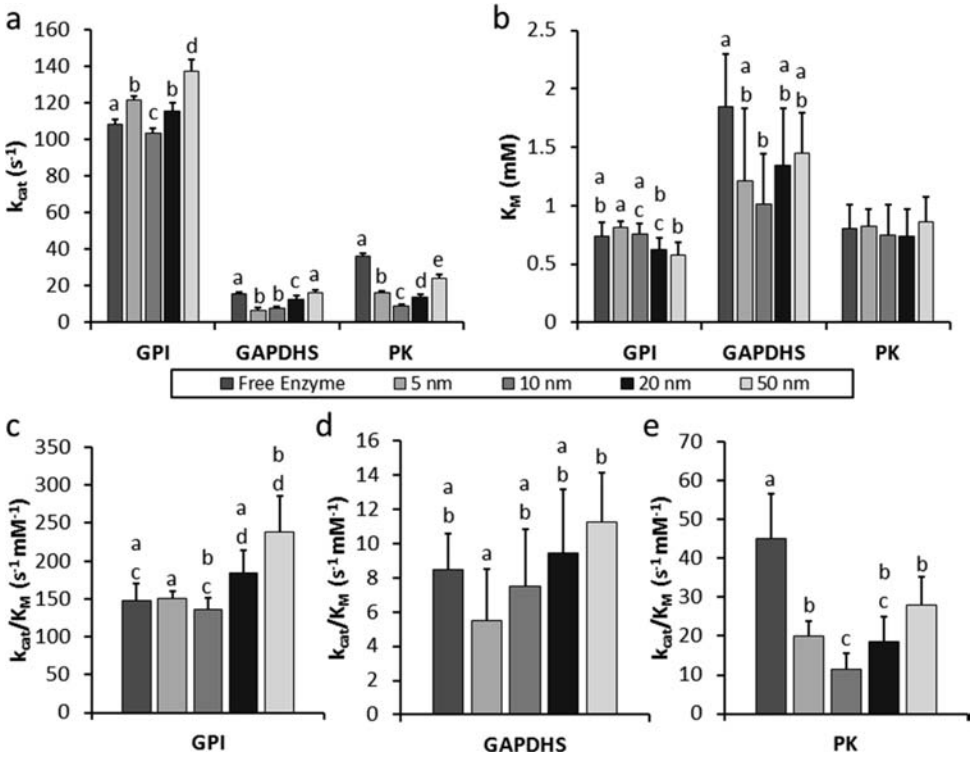

Figure 2. Kinetics of the tethered enzymes in a monolayer. Activity was measured for each enzyme on various sizes of AuNP with varying amounts of substrate. Values for k_{cat} and K_M were calculated using Michaelis−Menten kinetics. (a) The turnover number (k_{cat}) displayed no significant trend, irrespective of enzyme type. (b) K_M also showed no significant difference for any enzyme as the size of AuNP changed. (c−e) Both kinetic variables were then utilized to plot enzyme efficiency (k_{cat}/K_M) yielding no clear trend for change in efficiency as AuNP size increased. Error bars show standard deviation. All comparisons among sizes for a given enzyme were performed using a Student's *t* test with unequal variance (*Excel*); dissimilar letters denote significance at $p < 0.05$, no letters indicate no significance.

upon attachment chemistry, and not an inherent impact of NP size on tethered enzyme activity.

Last, we looked at k_{cat}/K_M, reflecting the efficiency with which an enzyme converts a substrate to product. All three enzymes showed slight yet statistically significant differences in k_{cat}/K_M with differing NP sizes, largely reflecting the variation in k_{cat}. However, no clear trends were observed. Notably, the fact that there were only subtle changes in any of the three kinetic variables when enzymes were tethered to different sizes of NPs in a monolayer emphasizes the advantages of a tethering strategy based on oriented immobilization.

Next, we investigated the impact of NP size under conditions of maximum enzyme loading which yields maximum activity per AuNP. To test maximal enzyme binding and multilayer formation per NP, an excess of each enzyme was incubated with NTA-AuNPs of each size (SI Figure 8) and then washed repeatedly. Amounts of enzyme bound (Figure 3a) were measured with BCA assays (SI Figure 9). Surface area calculations (using spherical approximations for the functional multimers) and measured amounts of enzyme bound were used to calculate multilayer formations (Figure 3b). These calculations were corroborated empirically using TEM on NTA-AuNPs with tethered GPI (Figure 3c−g). Our results showed that enzyme multilayers increased as NP size increased.

The multilayer conjugates displayed significant trends in specific activity and the kinetic variables. Activity per NP increased with increasing NP size when compared to monolayer results, and as expected, the larger AuNPs with more multilayers displayed higher activity than those on the small AuNPs (Figure 4). Final kinetics and Pearson correlation factors (CF) to show trends with increasing NP size are shown in Figure 5 and Table 1. When tethered, each enzyme showed a significant, decreasing trend in k_{cat} with increasing AuNP size, with an average CF of 0.9. One possible explanation is that the increased number of multilayers on the larger NPs decreased the effective amount of active enzyme on the larger particles; this is modeled and discussed below. A comparison with the monolayer data supports this hypothesis.

Much like the monolayer data, K_M showed no significant trends in multilayer data. Again, this is most likely due to our tethering strategy which might orient enzyme complexes even in layers at a distance from the surface of the NP, due to the positively charged his-tag. All three enzymes showed a decrease in enzyme efficiency as AuNP size increased (CF: 0.96 for GPI; 0.88 for GAPDHS; 0.86 for PK), primarily due to the changes in k_{cat}. Importantly, it is worth noting that there was 73−94% retention of enzyme specific activity when comparing the enzymes with maximum efficiency (tethered to the 5 nm AuNP) with untethered counterparts (SI Figure 10). This very high activity highlights the efficacy of our biomimetic tethering strategy; tethering via a specific domain helps prevent the enzymes from coming into direct contact with the surface. However, as discussed below, decreases in specific activity for larger sizes of NP were likely induced by enzyme multilayers.

Our data suggest that changes in enzyme kinetics primarily resulted from multilayer enzyme effects. As NP size increased, the number of enzyme multilayers increased. The reasoning behind why multilayers form on larger NPs is not entirely known; however, we hypothesize that several factors could have contributed. First, as the curvature of the particle decreased

DOI: 10.1021/acs.bioconjchem.5b00354
Bioconjugate Chem. 2015, 26, 1931−1938

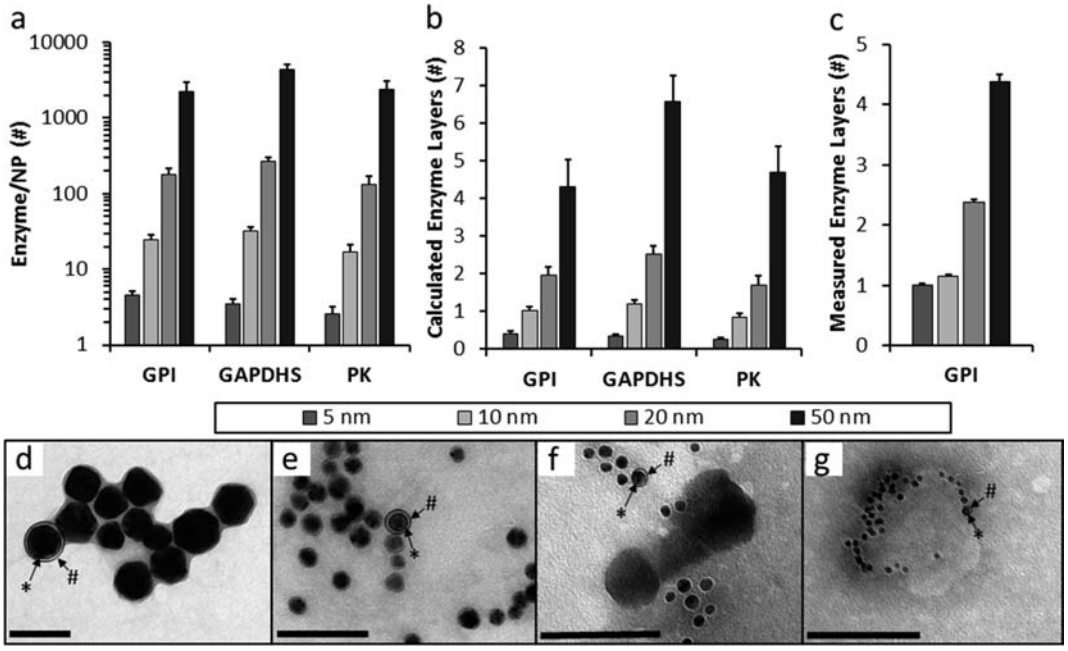

Figure 3. Binding and multilayer results for enzymes on NTA-AuNPs. (a) The amount of protein bound was calculated from measurements of total protein minus unbound protein and is plotted as the number of enzymes per NP for the three enzymes (GPI, GAPDHS, PK) on four sizes of AuNPs (⌀5, 10, 20, and 50 nm). (b) Based on the diameter of each enzyme as a functional multimer (assuming a spherical shape), and the AuNP surface area, we calculated the number of enzyme layers per NP. (c) For GPI, we then verified our calculated number of layers by measuring the thickness of the protein shells around each NTA-AuNP using TEM with negative staining. In the images of GPI tethered to the different sized NTA-AuNPs [50 nm (d), 20 nm (e), 10 nm (f), and 5 nm (g)], the protein shell appears gray (#, outer circle, outlined in black for one NP in each panel) around each black NTA-AuNP (*, inner circle). The shell was noticeably larger in the case of the 50 nm AuNPs compared to the smaller AuNPs. Scale bars are 100 nm. Error bars reflect standard errors of the mean (SEM). Comparisons among sizes for a given enzyme were performed using a Student's *t* test with unequal variance (*Excel*), and all are significant at $p < 0.05$.

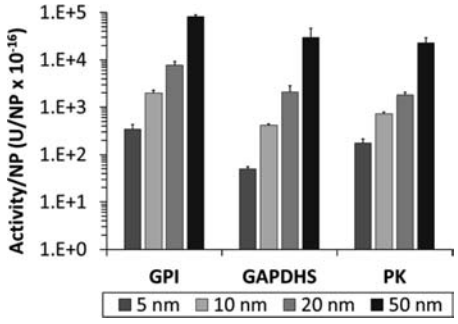

Figure 4. Total activity of multilayer tethered enzymes per NTA-AuNP. Enzymatic activity was measured for each size of functionalized AuNP and divided by the total number of AuNPs to give information about the activity per AuNP, which logarithmically increased as AuNP size increased. Error bars reflect standard deviation. All comparisons among sizes for a given enzyme were performed using a Student's *t* test with unequal variance (*Excel*), and are all significant at $p < 0.05$.

with increasing size, the distance between enzymes would also decrease. This would allow for closer packing on the surface, creating multilayers more readily than enzymes having to interact with more widely spaced and mobile enzymes on a highly curved surface. Second, the packing of enzymes in multilayers is likely controlled by weak protein−protein electrostatic forces. Due to our oriented immobilization strategy, there exists a highly positive his-tag present on each enzyme, which will be attracted to the negatively charged residues on lower enzyme layers. While increasing multilayers, this will also preserve a degree of orientation throughout the multilayers. The third possible cause for increased enzyme multilayers on large NPs is enzyme crowding.[24,25] At high enzyme concentrations it has been shown that enzymes prefer to form protein complexes with each other in order to minimize negative space. The enzyme crowding also stabilizes the enzymes by forcing them to remain in their folded state, which is more compact in crowded conditions, rather than their denatured state.

Although enzyme crowding and retention of enzyme orientation would enhance enzyme activity, there are also negative effects associated with multilayers. Steric hindrance between enzymes might impede needed conformational changes in lower enzyme layers. Also, the lower enzyme layers would not have ready access to substrate; adjacent enzymes would compete for any substrate which does penetrate through the layers. These negative effects would be lessened in the outermost layer of enzymes.

We investigated potential effects of multilayers on our kinetic parameters by calculating the number of enzymes in the outermost layer and assuming those were the only active enzymes (SI Figure 11). This assumption likely resulted in an underestimation of active enzymes because we deliberately did not take into account the activity of inner layers or how layers interact functionally. Middle layers may induce steric hindrance, be bound in nonoriented fashion, or conversely, may enhance activity by creating enzyme complexes. Differences in kinetic values with different NP sizes were not as prominent when only the outermost layer was presumed active; however, k_{cat} and k_{cat}/K_M decreased slightly for PK as NP size increased (Figure 6). The concordance of the results of this modeling with our measured results in Figure 2, even under the strict assumption that only the outermost layer might be active, suggests that the

DOI: 10.1021/acs.bioconjchem.5b00354
Bioconjugate Chem. 2015, 26, 1931−1938

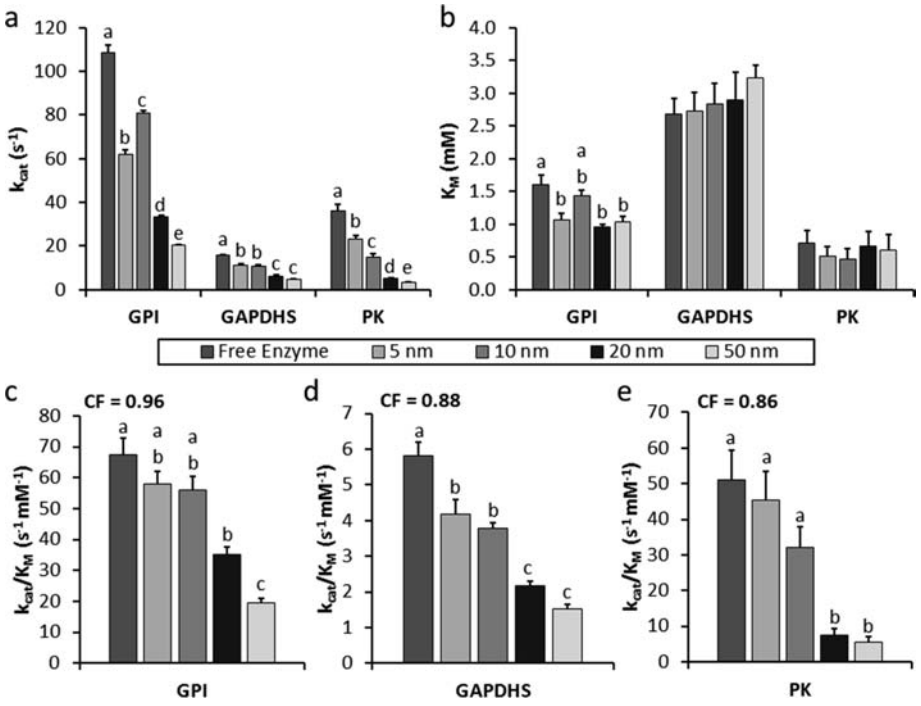

Figure 5. Graphical representation of the kinetics of the multilayer tethered enzymes. Activity was measured for each enzyme on various sizes of AuNP with varying amount of substrate. Values for k_{cat} and K_M were calculated using Michaelis–Menten kinetics. (a) The turnover number (k_{cat}) decreased as AuNP size increased, irrespective of enzyme type. (b) However, K_M showed no significant difference for any enzyme as the size of AuNP changed. (c–e) Both kinetic variables were then utilized to plot enzyme efficiency (k_{cat}/K_M) yielding a substantial decrease in efficiency as AuNP size increased with correlation factors as high as 0.96 for GPI. Error bars show standard deviation. All comparisons among sizes for a given enzyme were performed using a Student's *t* test with unequal variance (*Excel*); dissimilar letters denote significance at $p < 0.05$, no letters indicate no significance. Pearson's correlation factors (CF) were calculated using *Excel*.

Table 1. Effect of AuNP Size on Multilayer Tethered Enzyme Kinetics[a]

	AuNP Size	free enzyme	5 nm	10 nm	20 nm	50 nm
k_{cat} (s^{-1})	GPI	108.5 ± 3.26	62.1 ± 1.67	80.7 ± 1.39	33.5 ± 0.40	20.2 ± 0.54
	GAPDHS	15.7 ± 0.55	11.4 ± 0.48	10.7 ± 0.48	6.3 ± 0.37	4.9 ± 0.12
	PK	36.1 ± 3.00	23.1 ± 1.88	15.1 ± 1.22	5.0 ± 0.55	3.3 ± 0.41
K_M (mM)	GPI	1.61 ± 0.15	1.07 ± 0.10	1.44 ± 0.08	0.95 ± 0.04	1.03 ± 0.10
	GAPDHS	2.68 ± 0.24	2.72 ± 0.29	2.83 ± 0.31	2.90 ± 0.42	3.24 ± 0.19
	PK	0.71 ± 0.14	0.51 ± 0.16	0.47 ± 0.15	0.67 ± 0.22	0.60 ± 0.24
k_{cat}/K_M (s^{-1} mM^{-1})	GPI	67.4 ± 6.45	58.1 ± 5.55	56 ± 3.17	35.2 ± 1.54	19.6 ± 1.89
	GAPDHS	5.8 ± 0.56	4.2 ± 0.48	3.8 ± 0.45	2.2 ± 0.34	1.5 ± 0.10
	PK	50.9 ± 14.85	45.4 ± 14.13	32.1 ± 10.81	7.5 ± 2.60	5.5 ± 2.31

[a]Each measurement was carried out in triplicate from at least two separate preparations of each protein. Data were analyzed using *GraphPad Prism 6* software. Errors show standard deviation.

site-specific, oriented immobilization of the enzymes attaching to the NP conferred some beneficial impact that extended through the multilayers. This is consistent with our prior findings showing the advantage of this approach in terms of specific activity over random adsorption or carboxyl-amine binding.[16,17]

In summary, we used genetically encoded tags to provide site-specific immobilization of enzyme from three different classes on four sizes of NTA-AuNPs. As NP size increased, the amount of enzyme multilayers increased, as did enzymatic activity per NP. Monolayer data demonstrated the effectiveness of our tethering strategy, exhibiting negligible influence on the kinetics of the enzymes when attached to different sizes of AuNPs. Enzymatic activity (k_{cat} and k_{cat}/K_M) from multilayer data displayed negative trends as AuNP size increased, independent of enzyme class, whereas there was no change in K_M. Our data address the fundamental question of how NP size affects the kinetics and multilayer formation of varying enzyme classes in both monolayers as well as at maximal enzyme loading. Regardless of enzyme class, the larger particles showed higher total activity per NP, whereas smaller particles showed higher activity per enzyme molecule. These generalizable trends will be of value when designing diverse applications that utilize NPs functionalized with tethered enzymes.

MATERIALS AND METHODS

All materials and reagents were purchased from Sigma-Aldrich (MO, USA) or ThermoFisher Scientific (MA, USA) unless otherwise stated.

AuNP Surface Modifications. AuNPs prepared with a tannic acid/citrate reduction protocol were purchased from Sigma-Aldrich. All modifications of AuNPs were carried out in

DOI: 10.1021/acs.bioconjchem.5b00354
Bioconjugate Chem. 2015, 26, 1931–1938

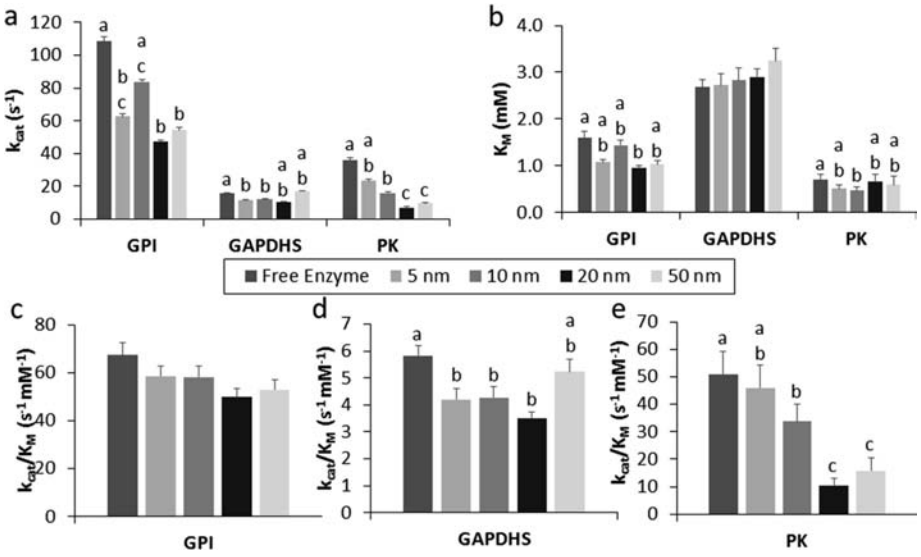

Figure 6. Comparison of the multilayer kinetics with respect to the outermost layer of tethered enzymes. Based on the modeled numbers of enzymes in the outermost layers, and assuming that only these enzymes were active, we saw surprisingly small change versus the results shown earlier in Figure 2. (a) The turnover number (k_{cat}) declined less sharply due to the decrease of effectively active enzymes for larger sizes of AuNPs, and was flat for the least active enzyme, GAPDHS. (b) The K_M was not influenced by the amount of effective enzymes and so did not change. (c−e) Consistent with the change in k_{cat}, enzyme efficiency (k_{cat}/K_M) also showed a less marked decrease in efficiency with increasing AuNP size. Error bars show standard deviation. Comparisons among sizes for a given enzyme were performed using a Student's *t* test with unequal variance (*Excel*); dissimilar letters denote significance at $p < 0.05$, no letters indicate no significance.

0.1 mM PBS solution. AuNPs were incubated with 11-mercaptoundecanoic acid (0.1 mg/mL dissolved in 95% ethanol) for 24 h at room temperature. Then, 10 μL of NaCl (2 M) were added every 30 min, for a total of three additions, and incubated for 3 h on a rocker at room temperature. Modified AuNPs were then washed three times by centrifugation (16 000 g for 20 min at 4 °C) and resuspension in 0.1 mM PBS. The carboxyl groups were activated with 1-ethyl-3-(3-(dimethylamino)propyl) carbodiimide (EDC 0.5 mg/mL) and *N*-hydroxysuccinimide (NHS 0.2 mg/mL) solution incubated at room temperature for 1 h. This mixture was then centrifuged and the AuNPs washed three times with 0.1 mM PBS. Next, *N,N*-bis(carboxymethyl)-L-lysine hydrate (NTA 0.5 mg/mL) was added to the AuNPs and incubated for 3 h at room temperature. This derivative of NTA includes an additional amine group which can react with the carboxyl groups on the surface. Then $NiCl_2$ (0.5 mg/mL) was added to the mixture to chelate the NTA. After 1 h, the NTA-AuNPs were washed three times by centrifugation and resuspension into 0.1 mM PBS. The AuNPs were characterized before and after Ni-NTA modification using SEM (MIRA3 LM FESEM, Tescan) with backscatter electron detection at an acceleration voltage of 10 kV for 50, 20, and 10 nm AuNPs and 30 kV for 5 nm AuNPs (SI Figure 1). A Zetasizer ZS (Malvern) was used to measure zeta potential distributions before and after Ni-NTA modification (SI Figure 2).

Functionalizing AuNPs with Tethered Enzymes. Recombinant GPI and GAPDHS were generated and their identity, relative purity, and activities verified using our previous methods.[16,17] Recombinant PK was generated from mouse testis RNA using the same methodology. Each recombinant enzyme was diluted to a working concentration of 0.1 mg/mL. Tethering was performed by incubating at 4 °C for 1 h using 30 μL of enzyme with 150 μL of NTA-AuNP (~4×10^{12} nm^2/μL), for each of the four sizes, or 20 μL of enzyme with 20 μL of NTA-AuNP (OD = 1), for monolayer and multilayer experiments, respectively. The NTA-AuNPs with bound enzymes were then washed three times with 0.1 mM PBS with final resuspension in 120 μL (monolayer), or 40 μL (multilayer), of 0.1 mM PBS. Amount of protein bound was calculated by subtraction of the unbound from the total (SI Figures 5 and 9). GPI tethered to NTA-AuNPs, using the multilayer approach, was evaluated using TEM (Tecnai 12 Bio-Twin TEM, FEI) at 120 kV (Figure 3d−g) with a phosphotungstic acid negative stain; the enzyme layers were measured using *ImageJ* (NIH). In calculating multilayers for each NP size, the enzyme thickness was normalized to the 5 nm NP's enzyme thickness, which was assumed to be a monolayer and which was corroborated by geometric calculations below. This took into consideration drying effects in sample preparation for TEM.

Calculations for Enzyme Layers. Enzyme size was estimated using similar crystal structures of each functional multimer taken from the RCSB Protein Data Bank (GPI from mouse: 1U0E, GAPDH from rabbit: 1J0X, PK from rabbit: 1F3W). We utilized spherical approximations for each multimer (GPI: 43.92 nm^2, GAPDHS: 56.76 nm^2, PK: 104.00 nm^2). The contact points of adjacent multimers were assumed to be spaced at the diameter of a multimer. To calculate the surface area of the first layer at the contact points, we used the radius of the NP plus the radius of the multimer (e.g., using a 5 nm NP and GPI, the radius for the surface area is 6.2 nm). This result was then multiplied by the number of NPs used to yield the total surface area of the first layer on all NPs. We divided the cross-sectional area of each multimer by the total surface area to yield the number of multimers that fit on the first layer. For each subsequent layer, the radius for surface area increases by the diameter of one multimer. To determine the number of layers for each enzyme and each size, we repeated this process until each model contained enough enzyme to match the measured amounts of protein bound to each NTA-AuNP. To

DOI: 10.1021/acs.bioconjchem.5b00354
Bioconjugate Chem. 2015, 26, 1931−1938

validate this modeling, the relative number of layers per size NP was confirmed empirically using TEM as described above.

Because larger NPs had more multilayers, they would be numerically disadvantaged in terms of specific activity, k_{cat}, and enzyme efficiency if their inner layers of multimers had restricted access to substrate. To investigate the impact on kinetic values of these enzymes in the underlying layers, we performed calculations using the assumption that only the "outer layer" of multimers were active. We defined "outer layer" to include all enzymes in the layer farthest away from the NP and the percentage of the second to last multimer layer which would not be covered by enzymes lying immediately atop them. For example, if only 60% of the top layer were occupied by multimers, then approximately 40% of the layer underneath would still have access to substrate.

Enzyme Activity Assays. Reactions were carried out in clear 96-well plates and absorbance (340 nm) was detected with a spectrophotometer (Infinite 200 PRO Plate Reader, Tecan). His-tagged enzyme constructs were used in the first step of each respective reaction and exogenous enzymes, substrates, and cofactors were added for quantification of activity. Kinetic assays used the following substrate concentrations: GPI, fructose 6-phosphate [0, 0.33, 0.67, 1.33, 2.67, 5.33, 10.67 mM]; GAPDHS, glyceraldehyde 3-phosphate [0, 0.3, 0.6, 1.25, 2.5, 5, 10 mM]; PK, phosphoenolpyruvate [0, 0.17, 0.33, 0.83, 1.67, 3, 6]. k_{cat} was calculated by dividing V_{max} by the concentration of enzyme bound (V_{max}/[E]). K_M was the substrate concentration at half V_{max}.

GPI was detected using the following reactions:

$$\text{Fructose 6-phosphate} \overset{\text{His-GPI}}{\rightleftharpoons} \text{Glucose 6-phosphate}$$

$$\text{Glucose 6-phosphate} + \text{NADP}^+ \overset{\text{G6PDH}}{\rightleftharpoons} \text{6-phospho-D-glucono-1,5-lactone} + \text{NADPH} + \text{H}^+$$

GAPDHS was detecting using the following reactions:

$$\text{Glyceraldehyde 3-phosphate} + \text{NAD}^+ \overset{\text{His-GAPDHS}}{\rightleftharpoons} \text{1,3-bisphosphoglycerate} + \text{NADH} + \text{H}^+$$

$$\text{1,3-bisphosphoglycerate} + \text{ADP} \overset{\text{PGK}}{\rightleftharpoons} \text{3-phosphoglycerate} + \text{ATP}$$

PK was detected using the following reactions:

$$\text{Phosphoenolpyruvate} + \text{ADP} \xrightarrow{\text{His-PK}} \text{Pyruvate} + \text{ATP}$$

$$\text{Pyruvate} + \text{NADH} \overset{\text{LDH}}{\rightleftharpoons} \text{Lactate} + \text{NAD}^+$$

■ ASSOCIATED CONTENT

Supporting Information

The Supporting Information is available free of charge on the ACS Publications website at DOI: 10.1021/acs.bioconjchem.5b00354.

AuNP characteristics, protein binding results, secondary enzyme activities, activity per AuNP of monolayer enzymes, specific activity of multilayer enzymes, calculated amount of multilayer functional enzymes, and a table on prior studies in the field (PDF)

■ AUTHOR INFORMATION

Corresponding Author

*E-mail: ajt32@cornell.edu.

Author Contributions

J.P.L., L.G., and A.J.T. conceived the experiments. L.G. produced preliminary data and optimized surface modification. J.P.L. performed the experiments and data analysis. L.A. and S.C. produced the TEM images. C.M. and R.C. engineered and optimized His-tagged enzymes and coupled reaction pathways. J.L.N. purified the enzymes and optimized enzyme protocols. J.P.L. and A.J.T. wrote the manuscript. All authors discussed the results, and read and revised the manuscript.

Notes

The authors declare no competing financial interest.

■ ACKNOWLEDGMENTS

This work was primarily supported by an NIH Pioneer Award (8DP1-EB016541; A.J.T.). This work made use of the Cornell Center for Materials Research Shared Facilities, which are supported through the NSF MRSEC program (DMR-1120296) and the Nanobiotechnology Center shared research facilities at Cornell.

■ REFERENCES

(1) Schoemaker, H. E. (2003) Dispelling the myths– Biocatalysis in industrial synthesis. *Science 299*, 1694−1697.

(2) Demin, S., and Hall, E. A. H. (2009) Breaking the barrier to fast electron transfer. *Bioelectrochemistry 76*, 19−27.

(3) Zebda, A., Gondran, C., Le Goff, A., Holzinger, M., Cinquin, P., and Cosnier, S. (2011) Mediatorless high-power glucose biofuel cells based on compressed carbon nanotube-enzyme electrodes. *Nat. Commun. 2*, 370.

(4) Arruda, D. L., Wilson, W. C., Nguyen, C., Yao, Q. W., Caiazzo, R. J., Talpasanu, I., Dow, D. E., and Liu, B. C. S. (2009) Microelectrical sensors as emerging platforms for protein biomarker detection in point-of-care diagnostics. *Expert Rev. Mol. Diagn. 9*, 749−755.

(5) Yoo, H. S., Kim, T. G., and Park, T. G. (2009) Surface-functionalized electrospun nanofibers for tissue engineering and drug delivery. *Adv. Drug Delivery Rev. 61*, 1033−1042.

(6) Fischer, T., and Hess, H. (2007) Materials chemistry challenges in the design of hybrid bionanodevices: supporting protein function within artificial environments. *J. Mater. Chem. 17*, 943.

(7) Halliwell, C. M., Morgan, G., Ou, C.-P., and Cass, A. E. G. (2001) Introduction of a (poly)histidine tag in l-lactate dehydrogenase produces a mixture of active and inactive molecules. *Anal. Biochem. 295*, 257−261.

(8) Popat, A., Hartono, S. B., Stahr, F., Liu, J., Qiao, S. Z., and Qing Lu, G. (2011) Mesoporous silica nanoparticles for bioadsorption, enzyme immobilisation, and delivery carriers. *Nanoscale 3*, 2801.

(9) Kim, J., Grate, J. W., and Wang, P. (2006) Nanostructures for enzyme stabilization. *Chem. Eng. Sci. 61*, 1017−1026.

(10) Bower, C. K., Sananikone, S., Bothwell, M. K., and McGuire, J. (1999) Activity losses among T4 lysozyme charge variants after adsorption to colloidal silica. *Biotechnol. Bioeng. 64*, 373−376.

(11) Vertegel, A. A., Siegel, R. W., and Dordick, J. S. (2004) Silica nanoparticle size influences the structure and enzymatic activity of adsorbed lysozyme. *Langmuir 20*, 6800−6807.

(12) Czeslik, C., and Winter, R. (2001) Effect of temperature on the conformation of lysozyme adsorbed to silica particles. *Phys. Chem. Chem. Phys. 3*, 235−239.

(13) Jia, H., Zhu, G., and Wang, P. (2003) Catalytic behaviors of enzymes attached to nanoparticles: the effect of particle mobility. *Biotechnol. Bioeng. 84*, 406−414.

(14) Wu, C.-S., Lee, C.-C., Wu, C.-T., Yang, Y.-S., and Ko, F.-H. (2011) Size-modulated catalytic activity of enzyme−nanoparticle

DOI: 10.1021/acs.bioconjchem.5b00354
Bioconjugate Chem. 2015, 26, 1931−1938

conjugates: a combined kinetic and theoretical study. *Chem. Commun. 47*, 7446.
(15) Park, H. J., McConnell, J. T., Boddohi, S., Kipper, M. J., and Johnson, P. A. (2011) Synthesis and characterization of enzyme−magnetic nanoparticle complexes: effect of size on activity and recovery. *Colloids Surf., B 83*, 198−203.
(16) Mukai, C., Gao, L., Bergkvist, M., Nelson, J. L., Hinchman, M. M., and Travis, A. J. (2013) Biomimicry enhances sequential reactions of tethered glycolytic enzymes, TPI and GAPDHS. *PLoS One 8*, e61434.
(17) Mukai, C., Bergkvist, M., Nelson, J. L., and Travis, A. J. (2009) Sequential reactions of surface-tethered glycolytic enzymes. *Chem. Biol. 16*, 1013−1020.
(18) Hainfeld, J. F., Liu, W., Halsey, C. M. R., Freimuth, P., and Powell, R. D. (1999) Ni-NTA Au clusters target his-tagged proteins. *J. Struct. Biol. 127*, 185−198.
(19) Yu, C.-C., Kuo, Y.-Y., Liang, C.-F., Chien, W.-T., Wu, H.-T., Chang, T.-C., Jan, F.-D., and Lin, C.-C. (2012) Site-specific immobilization of enzymes on magnetic nanoparticles and their use in organic synthesis. *Bioconjugate Chem. 23*, 714−724.
(20) Miki, K., Qu, W., Goulding, E. H., Willis, W. D., Bunch, D. O., Strader, L. F., Perreault, S. D., Eddy, E. M., and O'Brien, D. A. (2004) Glyceraldehyde 3-phosphate dehydrogenase-S, a sperm-specific glycolytic enzyme, is required for sperm motility and male fertility. *Proc. Natl. Acad. Sci. U. S. A. 101*, 16501−16506.
(21) Rezwan, K., Studart, A. R., Voros, J., and Gauckler, L. J. (2005) Change of zeta potential of biocompatible collodiol oxide particles upon adsorption of bovine serum albumin and lysozyme. *J. Phys. Chem. B 109*, 14469−14474.
(22) Greenwood, R., and Kendall, K. (1999) Selection of suitable dispersants for aqueous suspensions of zirconia and titania powders using acoustophoresis. *J. Eur. Ceram. Soc. 19*, 479−488.
(23) Hanaor, D., Michelazzi, M., Leonelli, C., and Sorrell, C. C. (2012) The effects of carboxylic acids on the aqueous dispersion and electrophoretic deposition of ZrO2. *J. Eur. Ceram. Soc. 32*, 235−244.
(24) Phillip, Y., and Schreiber, G. (2013) Formation of protein complexes in crowded environments–from in vitro to in vivo. *FEBS Lett. 587*, 1046−52.
(25) Kuznetsova, I. M., Turoverov, K. K., and Uversky, V. N. (2014) What macromolecular crowding can do to a protein. *Int. J. Mol. Sci. 15*, 23090−140.

DOI: 10.1021/acs.bioconjchem.5b00354
Bioconjugate Chem. 2015, 26, 1931−1938